

Journal of Materials Chemistry A

Accepted Manuscript



This is an *Accepted Manuscript*, which has been through the Royal Society of Chemistry peer review process and has been accepted for publication.

Accepted Manuscripts are published online shortly after acceptance, before technical editing, formatting and proof reading. Using this free service, authors can make their results available to the community, in citable form, before we publish the edited article. We will replace this *Accepted Manuscript* with the edited and formatted *Advance Article* as soon as it is available.

You can find more information about *Accepted Manuscripts* in the [Information for Authors](#).

Please note that technical editing may introduce minor changes to the text and/or graphics, which may alter content. The journal's standard [Terms & Conditions](#) and the [Ethical guidelines](#) still apply. In no event shall the Royal Society of Chemistry be held responsible for any errors or omissions in this *Accepted Manuscript* or any consequences arising from the use of any information it contains.

Eu³⁺ post-functionalized nanosized metal-organic framework for cation exchange-based Fe³⁺-sensing in aqueous environment

Cite this: DOI: 10.1039/x0xx00000x

You Zhou^a, Hao-Hong Chen^b, Bing Yan^{*.a}

Received 00th January 2014,
Accepted 00th January 2014

DOI: 10.1039/x0xx00000x

www.rsc.org/

A novel strategy was demonstrated to fabricate luminescent lanthanide functionalized MOF by encapsulating Eu³⁺ cations in the pores of MIL-53-COOH (Al) nanocrystals. The Eu³⁺ incorporated sample shows excellent luminescence and good fluorescence stability in water due to the sensitization and protection provided by the parent framework. Subsequently, Eu³⁺ incorporated nanocrystals were developed as a highly selective and sensitive probe for detection of Fe³⁺ in aqueous solution. In addition, the possible sensing mechanism based on cation exchange between Fe³⁺ and the framework Al³⁺ in MIL-53-COOH (Al) was discussed in detail. This is the first example for detecting Fe³⁺ in aqueous solution based on a lanthanide functionalized nanoscale MOF. The good fluorescence stability in aqueous environment, the low detection limit and broad linear range, together with the nanoscale nature of this probe suggest it has the potential for intracellular sensing and imaging of Fe³⁺.

Introduction

Fe³⁺ ions are one of the essential elements for either humans or other living organisms on account of their significance in many biochemical processes and biological systems, such as the storage and transport of oxygen, muscle and brain function, immune and enzyme systems.¹ The deficiency and overload of Fe³⁺ will result in various physiological disorders.² Anemia, skin ailments, and insomnia can be caused by lack of Fe³⁺, while when serum Fe³⁺ is at levels exceeding the normal range, it will induce increased incidence of certain cancers and damage of organs like liver, heart, and kidneys.³ Therefore, the identification and quantification of Fe³⁺ is of great importance.

Metal-organic frameworks (MOFs), a class of crystalline hybrid materials formed by the connection of metal centers or clusters and organic linkers, have gathered immense attention due to their potential applications in gas storage,⁴ separation,⁵ catalysis,⁶ and drug delivery.⁷ Recently, significant progress has been made in the application of luminescent MOFs for sensing metal cations, small molecules, explosives, and vapors.⁸ The tunable intriguing structures and permanent porosity of luminescent MOFs make them well suited for developing fluorescence sensors. This is because the diverse pore topologies and accessible channels, functional sites (Lewis basic/acidic sites and open metal sites) produce their high selective recognition for analytes. In addition, the interactions between the framework and analytes may result in pre-concentration of analytes in the pores, thus giving rise to a lower detection limit and higher sensing sensitivity.

Among the diverse luminescent MOFs, lanthanide luminescent MOFs are especially attractive for fluorescence probes owing to their unique optical properties originating from the 4f electronic configuration of Lanthanides. These include large Stokes shifts, extremely sharp emission, long luminescence lifetimes (milliseconds) and high quantum yields when sensitized by efficient ligand-metal energy transfer (the so-called “antenna effects”). Up to date, a few luminescent lanthanide functionalized MOFs have been constructed for sensing of Fe³⁺.⁹ However, the luminescent lanthanide functionalized MOFs reported for Fe³⁺ detection are not in nanometer scale, and most of them are exploited as fluorescence sensor of Fe³⁺ in DMF solution due their poor stability in aqueous environment.⁹ Unfortunately, their large size and incompatibility with water tremendously hamper the practical sensing application in environmental and biological systems. To the best of our knowledge, the Fe³⁺ optical sensor with nanoscale nature and good water stability based on the lanthanide luminescence MOFs has never been reported. Besides, the rational design and preparation of desired lanthanide MOFs remain a great challenge because of the high coordination numbers and variable nature of the Ln³⁺ sphere.¹⁰

In this contribution, an alternative approach was demonstrated to fabricate a highly luminescence nanosized MOF by encapsulating Eu³⁺ cations in MIL-53-COOH (Al) (1) nanocrystals, which opens the way toward a new class of Lanthanide luminescence MOFs. What's more, the Eu³⁺ incorporated nanocrystals of 1 (Eu³⁺@1) was developed as a

highly selective and sensitive fluorescence probe targeting Fe^{3+} cations in aqueous solution. This luminescence probe is suitable for the detecting Fe^{3+} in environmental and biological systems. The possible sensing mechanism based on cation exchange was also discussed in detail.

Experimental section

Materials and measurements

All chemicals were commercially available and of reagent grade. Ultrapure water and ethanol was used throughout all experiment. $\text{AlCl}_3 \cdot 6\text{H}_2\text{O}$, trimellitic acid ($\text{H}_2\text{BDC}-\text{COOH}$) and N, N-dimethylformamide (DMF) were used to synthesize MIL-53-COOH (Al) (**1**). Europium chlorate was obtained from the Eu_2O_3 in HCl (37.5 %). Aqueous solutions of K^+ , Na^+ , Mg^{2+} , Ca^{2+} , Zn^{2+} , Co^{2+} , Ni^{2+} , Ag^+ , Pb^{2+} , Cr^{3+} , Fe^{3+} was prepared from nitrate salts; solutions of Cd^{2+} , Hg^{2+} was prepared from chlorate salts; Fe^{2+} solution was prepared from ferrous sulfate and used immediately. PXRD patterns were recorded with a Bruker D8 diffractometer using $\text{CuK}\alpha$ radiation with 40 mA and 40 kV. Transmission electron microscopy (TEM) was carried out on a JEOL JEM-2010F electron microscope and operated at 200 kV. Fourier transform infrared spectra (FTIR) were measured within KBr slices from 4000-400 cm^{-1} using a Nexus 912 AO446 infrared spectrum radiometer. Thermogravimetric analysis (TGA) was measured using a Netzsch STA 449C system at a heating rate of 5 K min^{-1} under the nitrogen protection. Nitrogen adsorption/desorption isotherms were measured at the liquid nitrogen temperature, using a Nova 1000 analyzer. The samples were outgassed for 3 h at 150 $^\circ\text{C}$ before the measurements. Surface areas were calculated by the Brunauer–Emmett–Teller (BET) method. ICPMS data were obtained on an X-7 series inductively coupled plasma-mass spectrometer (Thermo Elemental, Cheshire, UK). X-ray photoelectron spectra experiments were carried out on a RBD upgraded PHI-5000C ESCA system (Perkin Elmer) with Mg $\text{K}\alpha$ radiation ($h\nu = 1253.6 \text{ eV}$). The diffuse-reflectance UV-visible study was performed with a BWS003 spectrophotometer.

Synthesis of nanosized compound **1**

Nanoparticles of **1** was solvothermally synthesized from a mixture of aluminum chloride $\text{AlCl}_3 \cdot 6\text{H}_2\text{O}$, trimellitic acid, and DMF. The molar ratio of $\text{Al}^{3+} : \text{H}_2\text{BDC}-\text{COOH}$ is 1 : 1. The reactants were stirred a few minutes before transferring the resulting suspension to a Teflon-lined steel autoclave, and the temperature was set at 180 $^\circ\text{C}$ for 12 h. The resulting nanocrystals were separated from the mixed dispersion by centrifugation at 16000 rpm for 10 min. To remove the excess of unreacted trimellitic acid and aluminium chloride species, MIL-53-COOH (Al) nanoparticles were readily redispersed in absolute ethanol and centrifuged for three cycles. Finally, the product was dried at 60 $^\circ\text{C}$ for 6 h in vacuum (yield: about 85% based on Al).

Eu^{3+} @**1** preparation

Compound **1** (100 mg) was soaked in ethanol solutions of chlorate salts of Eu^{3+} (10 mL, 1 mmol). After two days of

soakage, the crystals were extensively washed with ethanol to remove residual Eu^{3+} cations on the surface. Subsequently, the resulted white powder was dried under vacuum at 60 $^\circ\text{C}$ for 6 h.

Sample Preparation for ICPMS studies

20 mg of Eu^{3+} @**1** nanocrystals was dispersed in a 10 mL Fe^{3+} solution with various concentrations (0-500 μM). As a control, 20 mg of Eu^{3+} @**1** was in parallel dispersed in 10 mL of ultrapure water without adding Fe^{3+} . After immersing for 5 min, nanocrystals of Eu^{3+} @**1** were removed by centrifugation (3 times, 16000 rpm). The filtrate was diluted to 20 mL and then introduced for ICPMS determination upon addition of 50 μL of nitric acid.

Luminescent Experiments

The luminescent spectra and the luminescent decay curves were obtained from an Edinburgh fluorescence spectrometer FLS920P using a μF920H pulsed xenon flashlamp. The luminescent properties were investigated in both the solid state and suspensions at room temperature. The outer absolute luminescent quantum efficiency was determined employing an integrating sphere (150 mm diameter, BaSO_4 coating) from Edinburgh FLS920 phosphorimeter. The quantum yield can be defined as the integrated intensity of the luminescence signal divided by the integrated intensity of the absorption signal. The excitation wavelength of the measurement of the emission quantum yields is 324 nm.

Luminescence responses of Eu^{3+} @**1** toward aqueous solution of various metal cations were investigated in their suspensions. The suspensions were prepared by dispersing Eu^{3+} @**1** powder (2 mg) into 5 mL aqueous solutions containing different metal cations (5 mM). The mixtures were then used for luminescence measurements. The luminescence data were collected after 5 min.

Results and discussion

Characterization of and Eu^{3+} @**1**

Nanocrystals of MOF **1** was solvothermally synthesized from a mixture of aluminum chloride $\text{AlCl}_3 \cdot 6\text{H}_2\text{O}$, trimellitic acid, and DMF. The PXRD pattern of the resulted product was indexed and refined using the Le Bail method (Figure 1). Table S1 gives an overview of the obtained lattice parameters, which are in good agreement with the ones previously reported.¹¹ The structure is built up from chains of trans- μ -OH corner-sharing AIO6 octahedra and terephthalate ions, creating a three-dimension framework with a one dimension pore channel system. TEM image (Figure S1) indicates the product is composed of irregularly shaped nanoparticles with the size in the range of 20-60 nm. The amalgam observed in TEM image probably consists of amorphous aluminum carboxylate, which may be originated from the degradation of the MOF, on the basis of MOFs are extremely sensitive to the electron beam used in TEM characterization, with their structures collapsing after a few minutes of exposure.¹² Afterward, compound **1** was immersed in ethanol solution of EuCl_3 for Eu^{3+} encapsulation. The number of Eu^{3+} cations that loaded in **1** has been

determined by ICPMS. It reveals the ratio of Al^{3+} and Eu^{3+} is close to 1 : 1 (1 : 0.83), suggesting one noncoordinating carboxyl group is incorporated with one Eu^{3+} cation. The nanocrystals of **1** maintain the crystalline integrity after incorporating Ln^{3+} cations, as demonstrated by the PXRD patterns shown in Figure S2. In addition, the morphology and size of these nanoparticles keep unchanged upon encapsulation of Eu^{3+} (Figure S3).

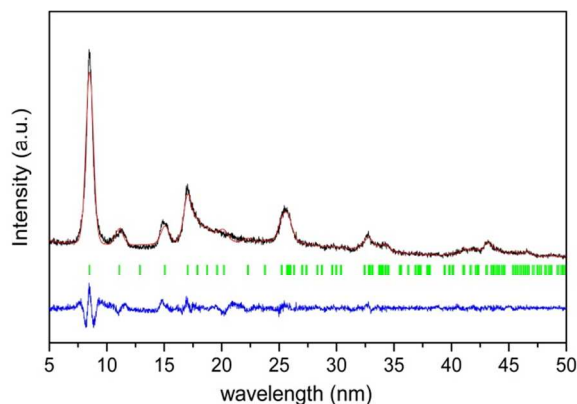


Figure 1 Le Bail fit of nanocrystals of MIL-53-COOH (Al).

The as-prepared $\text{Eu}^{3+}@1$ nanocrystals were also monitored by FTIR spectra, N_2 adsorption-desorption, and TG analysis. In the FTIR spectra (Figure S4), characteristic stretching vibrations of the coordinating carboxylate groups are easily visible, ν_{as} at 1600 and ν_{s} at 1430 and 1409 cm^{-1} . The presence of water molecules can be evidenced by the band with a maximum at 3420 cm^{-1} . The absorptions at 1130 and 778 cm^{-1} are ascribed to the C-H deformation vibrations of the aromatic ring, whereas the symmetric ring-stretching vibration emerges at 1497 cm^{-1} . N_2 adsorption-desorption isotherms of $\text{Eu}^{3+}@1$ is shown in Figure 2a. Unlike a type I adsorption curve, which commonly was seen in microporous materials, it displays typical a type IV curve with H1-type hysteresis loops at high relative pressure. The atypical hysteresis of these N_2 adsorption isotherms could be attributed to the steric hindrance of the free non-coordinated carboxyl groups within the channels, which reduces the access of N_2 molecules. The BET surface area of $\text{Eu}^{3+}@1$ is 286 $\text{m}^2 \text{g}^{-1}$, which shows reasonable reduction in comparison with the reported value of Al-MIL-53-COOH (393 $\text{m}^2 \text{g}^{-1}$) due to the encapsulation of Eu^{3+} .^{11b} The TGA (Figure 2b) data demonstrates $\text{Eu}^{3+}@1$ is thermally stable to 400 $^\circ\text{C}$, implying the good thermal stability of $\text{Eu}^{3+}@1$. The first weight loss occurs in the range of 50–170 $^\circ\text{C}$, which corresponds to the removal of the water molecules in the pores.

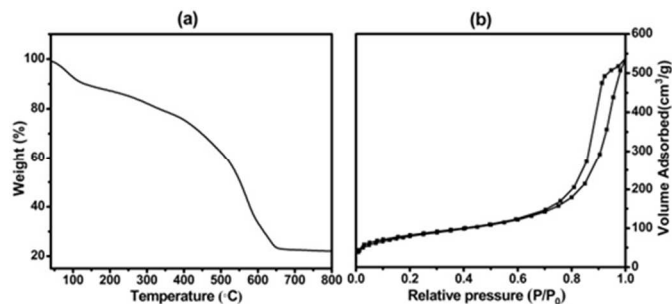


Figure 2 N_2 adsorption-desorption isotherms (a) and thermal gravimetric analysis (b) of $\text{Eu}^{3+}@1$.

Luminescence properties of $\text{Eu}^{3+}@1$

After post-synthetic functionalization of Eu^{3+} , the emission spectrum of the product exhibits characteristic emission of Eu^{3+} . The sharp lines centered at 579, 590, 616, 653, 701 nm can be ascribed to $^5\text{D}_0 \rightarrow ^7\text{F}_J$ ($J = 0-4$) transitions of Eu^{3+} .¹³ The 616 nm emission has maximum intensity, demonstrating that the incorporated Eu^{3+} ions occupy sites without an inversion center and have low crystal field symmetry.¹⁴ This is further confirmed by the presence of 579 nm emission, because this peak only occurs when Eu^{3+} symmetry is low.¹⁵ In addition, it is worth noted that the ligand-centered broad emission of compound **1** (Figure S5) can't be observed in the emission spectrum of $\text{Eu}^{3+}@1$, indicating the “antenna effect” occurs, that is, energy migration takes place upon ligand absorption, followed by intersystem crossing $\text{S}_1 \rightarrow \text{T}_1$ and antenna $\text{T}_1 \rightarrow \text{f}$ transfer, and then generating $\text{f} \rightarrow \text{f}$ emissions of Eu^{3+} cations. The excitation spectrum collected at the wavelength of 616 nm displays a dominating broad band in the range of 250–350 nm originated from the absorption of trimellitic acid ligands, providing a further evidence for the “antenna effect”. Moreover, $\text{Eu}^{3+}@1$ exhibits reasonable long lifetimes (0.45 ms) and high quantum yields (16%), which is attributed to the effective energy transfer from the ligand embedded in the framework to the encapsulated Eu^{3+} . From the above results, we can conclude that MOF **1** can serve as an efficient scaffold for hosting and sensitizing the luminescence of Eu^{3+} .

The luminescence properties of $\text{Eu}^{3+}@1$ nanocrystals in aqueous solution have also been investigated. The luminescence intensity of $\text{Eu}^{3+}@1$ suspension shows surprising little reduction as the time progress, implying the good day to day fluorescence stability in aqueous solution (Figure S6). These nanocrystals also exhibit good pH-independent luminescence stability in the pH range of 4–10 (Figure S7). The good stability of $\text{Eu}^{3+}@1$ emission in aqueous environment probably can be ascribed to the sufficient protection to Eu^{3+} provided by the MOF scaffold. The ability to compatible with aqueous environment, as well as the nanoscale nature of $\text{Eu}^{3+}@1$ particles makes them well suited for generating new fluorescence sensors in environmental and biological systems.¹⁶

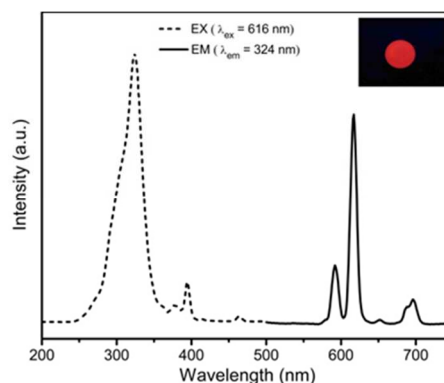


Figure 3 Excitation and emission spectra of $\text{Eu}^{3+}@1$. The inset is the corresponding picture under UV-light irradiation.

Sensing of Fe³⁺ cations

In the light of the excellent luminescence and good water stability of Eu³⁺@1, we examine the potential of Eu³⁺@1 for detecting metal cations. The luminescent responses of Eu³⁺@1 toward aqueous solutions of various metal cations are shown in Figure 4a. The metal cations, including which abundant in cells (K⁺, Na⁺, Mg²⁺, Ca²⁺, Cu²⁺) and present in trace quantities in living organisms (Zn²⁺, Co²⁺, Ni²⁺, Fe²⁺, Ag⁺), as well as toxic metals prevalent in environment (Hg²⁺, Cd²⁺, Pb²⁺, Cr³⁺), show slight influence on the emission intensity of Eu³⁺@1; however, only Fe³⁺ gives significant quenching effect on the luminescence. The remarkable quenching effect can be further confirmed by the photograph of Eu³⁺@1 suspension under UV light irradiation (Figure S8). The visible red light of Eu³⁺@1 suspension is essentially completely quenched when in contact with aqueous solution of Fe³⁺. The above results indicate the high selectivity of Eu³⁺@1 for the sensing and specific recognition of Fe³⁺ in aqueous environment.

In addition, the quenching effect of Fe³⁺ on the luminescence of Eu³⁺@1 was evaluated by fluorescence decay time of Eu³⁺ (Figure 4b). Most of the metal cations have negligible impact on the luminescence lifetime of Eu³⁺, while Cu²⁺ and Fe³⁺ exhibit varying degrees of decline in the fluorescence lifetime. Especially in the case of Fe³⁺, the decay time of Eu³⁺@1 is undetectable in the presence of 5 mM Fe³⁺. This observation agrees well with the responses of luminescence of Eu³⁺@1 towards various metal cations.

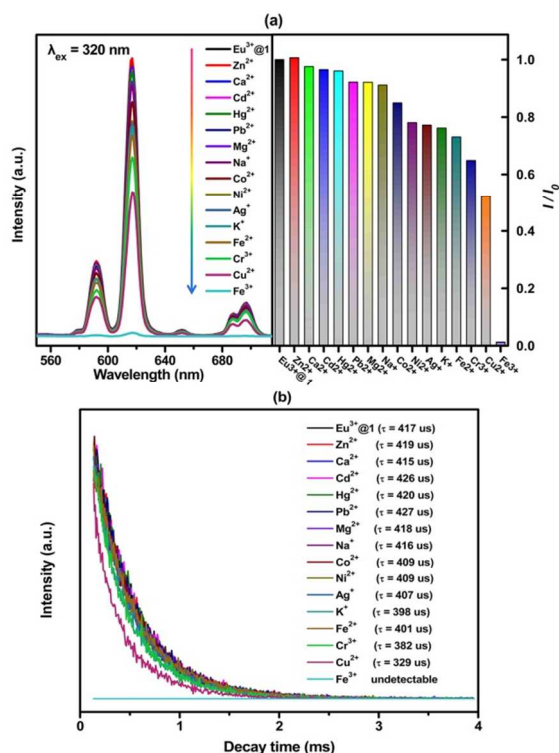


Figure 4 Responses of the fluorescence (a) and lifetime (b) of Eu³⁺@1 (0.4 mg L⁻¹) towards aqueous solution of various metal cations (5 mM). Both the emission spectra and lifetimes were collected at the excitation

wavelength of 320 nm. I and I₀ denote the fluorescence intensity of Eu³⁺@1 with and without metal ions of interest, respectively.

The influence of other metal cations (K⁺, Na⁺, Ag⁺, Ca²⁺, Mg²⁺, Cu²⁺, Zn²⁺, Co²⁺, Ni²⁺, Hg²⁺, Cd²⁺, Pb²⁺, Fe²⁺, Cr³⁺) on the detecting of Fe³⁺ was also determined. As can be seen from Figure 4a, the emission intensity of Eu³⁺@1 only shows slightly changes in the presence of other metal cations. Upon the introduction of Fe³⁺ to the mixture of Eu³⁺@1 and other metal cations, the fluorescence is significantly quenched (Figure 5). This reveals the interference from conventional metal cations can be neglected, further convincing the high selectivity of Eu³⁺@1 for Fe³⁺ detection and the potential of Eu³⁺@1 for practical use.

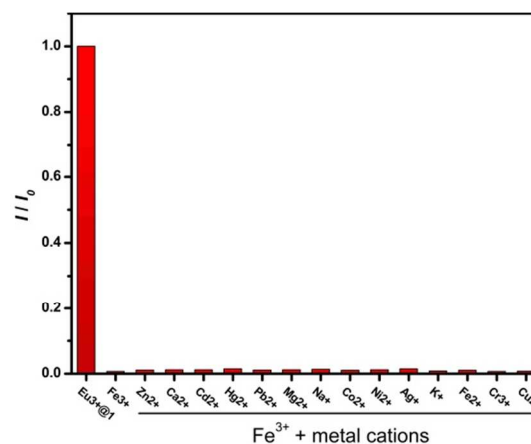


Figure 5 Luminescence intensity of Eu³⁺@1 (0.4 g L⁻¹) upon the addition of Fe³⁺ (5 mM) in the presence of background of metal cations (5 mM) in aqueous solution. λ_{ex} = 324 nm, λ_{em} = 616 nm.

For better understanding the response of fluorescence of Eu³⁺@1 to Fe³⁺ cations, the luminescence titration upon the addition of Fe(NO₃)₃ to Eu³⁺@1 was further conducted. As demonstrated in Figure 6a, the emission intensity of Eu³⁺@1 suspension declines sharply with the increase of Fe³⁺ concentration from 0 to 0.5 mM. Quantitatively, this quenching effect can be rationalized by the Stern–Volmer equation:

$$I_0/I = 1 + K_{sv} \times [Q] \quad (1)$$

where K_{sv} is the quenching constant, [Q] is the Fe³⁺ concentration, and the values I₀ and I are the luminescence intensity of Eu³⁺@1 suspension without and with addition of Fe³⁺, respectively.¹⁷ Figure 6b shows the K_{sv} curve of Eu³⁺@1 nanocrystals with Fe³⁺. The linear correlation coefficients (R) of is 0.99938, suggesting the quenching effect of Fe³⁺ on the luminescence of Eu³⁺@1 fits the Stern–Volmer model well. The K_{sv} value is calculated as 5.12 × 10³, which reveals a strong quenching effect on the Eu³⁺@1 luminescence. It is speculated that a static quenching process is dominate because the absorption spectrum of Eu³⁺@1 shows obvious difference after contacting with Fe³⁺ (Figure S10). The limits of detection for Fe³⁺ is determined as 0.5 μM, which is comparable to or better than some previously reported fluorescence sensor for Fe³⁺.²

^{9a,18} Furthermore, the low detection limit meets the requirements for intracellular sensing and imaging of Fe^{3+} .¹⁹

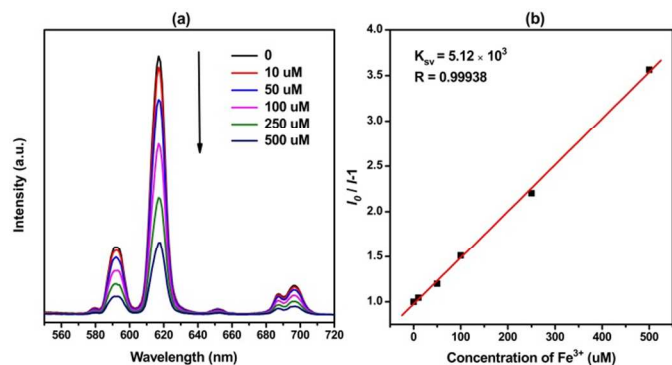


Figure 6 Emission spectra (a) and K_{sv} curve (b) of $\text{Eu}^{3+}@1$ (0.4 g L^{-1}) nanocrystals in aqueous solutions in the presence of various concentrations of Fe^{3+} under excitation at 320 nm.

The possible mechanism of luminescence quenching of $\text{Eu}^{3+}@1$ by Fe^{3+}

It has been reported that the quenching effect on luminescence of MOFs by metal cations can be originated from three approaches: 1) the interaction between metal cations and organic ligands;^{8d, 9c, 20} 2) the collapse of the crystal structure by metal cations;^{9b} 3) the cation exchange of central cations in framework with targeted cations.^{18a} Of particular relevance to the present work is the transformation of MIL-53 (Al) to MIL-53 (Fe) via cation exchange between Fe^{3+} and the framework Al^{3+} reported by Cheng and co-workers.^{18a} Inspired by this, we speculate the remarkable quenching effect of $\text{Eu}^{3+}@1$ by Fe^{3+} is resulted from the transformation of the parent framework MIL-53-COOH (Al) to MIL-53-COOH (Fe) via the cation exchange of Al^{3+} in $\text{Eu}^{3+}@1$ with Fe^{3+} .

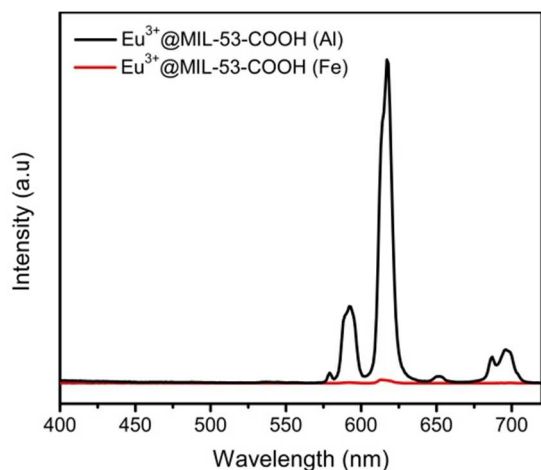


Figure 7 Emission spectra ($\lambda_{ex} = 324 \text{ nm}$) of $\text{Eu}^{3+}@1$ and $\text{Eu}^{3+}@MIL-53-COOH$ (Fe).

With the purpose of examining the hypothesis, the isomorphous MIL-53-COOH (Fe) with Fe^{3+} metal center was prepared for comparison. As we can't obtain the crystal of MIL-53-COOH (Fe) for single-crystal X-ray diffraction study, the PXRD was used to determine the structure of MIL-53-COOH (Fe). The PXRD result shows that the isomorphous MIL-

53-COOH (Fe) has been successfully synthesized (Figure S9). Subsequently, Eu^{3+} was introduced to MIL-53-COOH (Fe) forming $\text{Eu}^{3+}@MIL-53-COOH$ (Fe). The luminescence of $\text{Eu}^{3+}@MIL-53-COOH$ (Fe) is much weaker than $\text{Eu}^{3+}@1$ (Figure 7), implying the possibility of that the significant luminescence quenching of $\text{Eu}^{3+}@1$ by Fe^{3+} is caused by the cation exchange between Fe^{3+} and the framework Al^{3+} in $\text{Eu}^{3+}@1$.

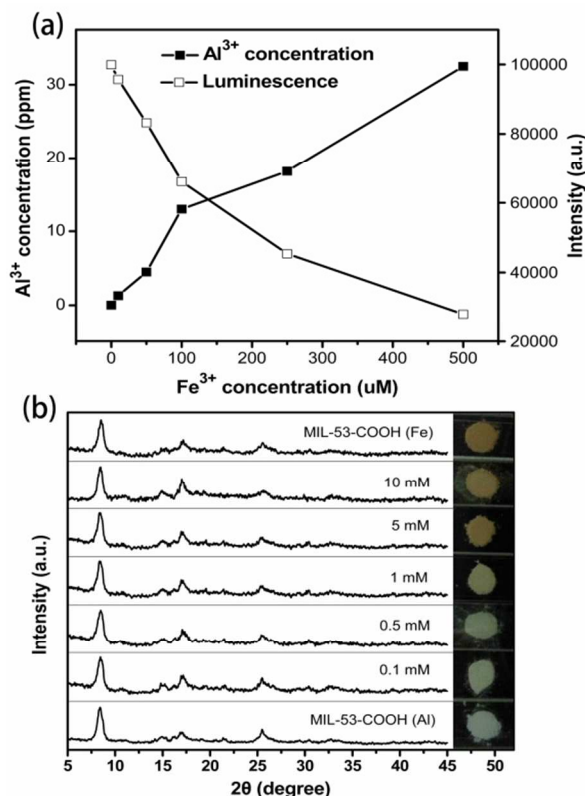


Figure 8 (a) Al^{3+} Concentrations of the filtrate solution of $\text{Eu}^{3+}@1$ upon addition of different contents of Fe^{3+} and the luminescence intensity of $\text{Eu}^{3+}@1$ as a function of the concentration of Fe^{3+} added. (b) PXRD patterns of the MIL-53(Al) after immersing in Fe^{3+} solution with various concentrations.

To verify the cation exchange between Fe^{3+} and Al^{3+} , 20 mg compound $\text{Eu}^{3+}@1$ was dispersed in 5 mL Fe^{3+} solution with various concentrations. After immersing for 30 min, the filtrates were introduced for ICPMS determination. Figure 8a illustrates the Al^{3+} concentration of the filtrate with different contents of added Fe^{3+} . The Al^{3+} concentration of the filtrated solution gradually increases as the level of Fe^{3+} elevates. It agrees well with the luminescence responses of $\text{Eu}^{3+}@1$ toward aqueous solutions of Fe^{3+} with various concentrations, implying the fluorescence quenching is resulted from the cation exchange mechanism. There is no doubt that the Al^{3+} cations are leached from 1. Either the framework collapse of MOF 1 or the cation exchange between Fe^{3+} and Al^{3+} can be responsible for the leaching of Al^{3+} . In order to clarify the origin of the leaching of Al^{3+} , the residues of mixed suspensions of $\text{Eu}^{3+}@1$ and Fe^{3+} were studied by PXRD. The results demonstrate that the framework remain its integrity after contact with Fe^{3+} , thus

ruling out the collapse of the framework (Figure 8b). This finding, together with the ICPMS results, suggests that Fe^{3+} cations exchanged the Al^{3+} in the parent framework and coordinated with the trimellitic acid ligand to maintain the framework. The photographs of the Fe^{3+} exchanged products also provide an indication that compound **1** gradually changed to MIL-53-COOH (Fe) as the concentration of Fe^{3+} increased (the inset in Figure 8b).

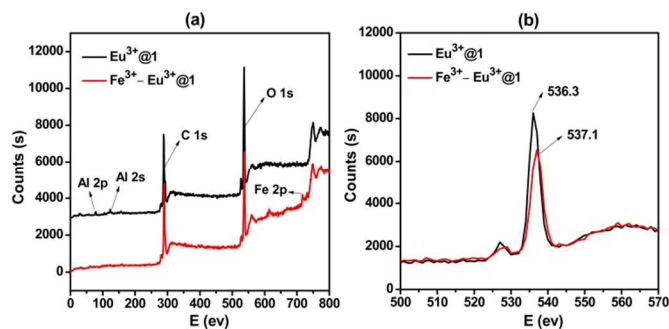


Figure 9 (a) XPS for $\text{Eu}^{3+}@1$ and $\text{Fe}^{3+}-\text{Eu}^{3+}@1$. (b) O 1s XPS for $\text{Eu}^{3+}@1$ and $\text{Fe}^{3+}-\text{Eu}^{3+}@1$. $\text{Fe}^{3+}-\text{Eu}^{3+}@1$ denotes the Fe^{3+} (5 mM) exchanged $\text{Eu}^{3+}@1$.

The cation exchange of framework Al^{3+} with Fe^{3+} was also monitored by XPS. As depicted in Figure 9, no obvious Al 2p and Al 2s peaks can be observed in the Fe^{3+} exchanged sample, while the of 2p for Fe^{3+} appears. This suggests that the cation exchange between framework Al^{3+} and Fe^{3+} occurred. Besides, the O 1s peak from $\text{Eu}^{3+}@1$ at 536.3 eV is shifted to 537.1 eV on the addition of Fe^{3+} , which indicates the original metal cation (Al^{3+}) coordinated to carboxyl group was substituted by Fe^{3+} . It further confirms the cation exchange of Al^{3+} in $\text{Eu}^{3+}@1$ to Fe^{3+} .

There remains a question as to why the strong luminescence of $\text{Eu}^{3+}@1$ almost completely quenched when the parent framework **1** transformed into MIL-53-COOH (Fe) through the cation exchange between Al^{3+} and Fe^{3+} . To elucidate this problem, we carried out the diffuse-reflectance UV-visible study of $\text{Eu}^{3+}@1$ and $\text{Fe}^{3+}-\text{Eu}^{3+}@1$. The results imply that the intense absorption of Fe^{3+} exchanged sample at the excitation wavelength is likely to be responsible for the observed quenching fluorescence (Figure S10). Because the strong absorption at excitation wavelength originated from ligand-metal charge transfer of $\text{O}^{2-}(\pi) \rightarrow \text{Fe}(3d)$ effectively suppresses the energy migration of excitation energy to Eu^{3+} through “antenna sensitization” process, which results in low populated emissive state of the incorporated Eu^{3+} cations and therefore significant luminescence quenching. The essentially unpopulated emissive state of Eu^{3+} can be verified by the undetectable decay time of the Fe^{3+} exchanged product (Figure 4b).

Conclusion

In summary, nanocrystals of **1** loaded with Eu^{3+} cations have been designed as a highly selective and sensitive fluorescence sensor for detecting Fe^{3+} in aqueous solution. This

luminescence probe of Fe^{3+} shows low detected limit (0.5) μM and broad linear range (0.5-500 μM). Moreover, the quenching effect of Fe^{3+} on $\text{Eu}^{3+}@1$ luminescence is not influenced in the presence of other conventional metal cation. The sensing mechanism is depending on the previously reported cation exchange of MOFs.^{9b, 21} The specific cation exchange behavior between the framework Al^{3+} in $\text{Eu}^{3+}@1$ and Fe^{3+} can cause effective suppression of the energy transfer from ligand to Eu^{3+} and therefore significant luminescence quenching of $\text{Eu}^{3+}@1$, thus allow $\text{Eu}^{3+}@1$ nanocrystals for highly selective detection of Fe^{3+} . The good fluorescence stability in aqueous environment, the low detection limit and broad linear range, together with the nanoscale nature of $\text{Eu}^{3+}@1$ suggest it has the potential for intracellular sensing and imaging of Fe^{3+} . The studies focus on $\text{Eu}^{3+}@1$ nanoparticles for Fe^{3+} intracellular sensing and imaging are currently under way.

Acknowledgements

This work was supported by the National Natural Science Foundation of China (91122003) and Developing Science Funds of Tongji University.

Notes and references

- ^a Department of Chemistry, Tongji University, Shanghai, 200092, China. E-mail: byan@tongji.edu.cn; Tel: +86-21-65984663
- ^b Shanghai Institute of Ceramics, Chinese Academy of Sciences, Shanghai 200050, China
- † Electronic Supplementary Information (ESI) available: [details of any supplementary information available should be included here]. See DOI: 10.1039/b000000x/
- (a) S. R. Lynch, *Nutr. Rev.*, 1997, **55**, 102; (b) L. M. Hyman and K. J. Franz, *Coord. Chem. Rev.*, 2012, **256**, 2333.
 - (a) P. Wu, Y. Li and X. P. Yan, *Anal. Chem.*, 2009, **81**, 6252; (b) Y. J. Ding, H. Zhu, X. X. Zhang, J. J. Zhu and C. Burda, *Chem. Commun.*, 2013, **49**, 7797.
 - T. N. Duc, R. El Zein, J. M. Raimundo, H. Dallaporta and A. M. Charrier, *J. Mater. Chem. B*, 2013, **1**, 443.
 - (a) L. J. Li, S. F. Tang, C. Wang, X. X. Lv, M. Jiang, H. Z. Wu and X. B. Zhao, *Chem. Commun.*, 2014, **50**, 2304; (b) A. R. Millward and O. M. Yaghi, *J. Am. Chem. Soc.*, 2005, **127**, 17998.
 - (a) Y. Q. Lan, H. L. Jiang, S. L. Li and Q. Xu, *Adv. Mater.*, 2011, **23**, 5015; (b) J. R. Li, R. J. Kuppler and H. C. Zhou, *Chem. Soc. Rev.*, 2009, **38**, 1477.
 - (a) Z. Y. Gu, J. Park, A. Raiff, Z. W. Wei and H. C. Zhou, *Chemcatchem*, 2014, **6**, 67; (b) V. Pascanu, Q. X. Yao, A. B. Gomez, M. Gustafsson, Y. F. Yun, W. Wan, L. Samain, X. D. Zou and B. Martin-Matute, *Chem. Eur. J.*, 2013, **19**, 17483.
 - (a) N. A. Vermeulen, O. Karagiari, A. A. Sarjeant, C. L. Stern, J. T. Hupp, O. K. Farha and J. F. Stoddart, *J. Am. Chem. Soc.*, 2013, **135**, 14916; (b) M. C. Bernini, D. Fairen-Jimenez, M. Pasinetti, A. J. Ramirez-Pastor and R. Q. Snurr, *J. Mater. Chem. B*, 2014, **2**, 766; (c) R. C. Huxford, J. Della Rocca and W. B. Lin, *Curr. Opin. Chem. Biol.*, 2010, **14**, 262.
 - (a) L. E. Kreno, K. Leong, O. K. Farha, M. Allendorf, R. P. Van Duyne and J. T. Hupp, *Chem. Rev.*, 2012, **112**, 1105; (b) B. L. Chen, S. C. Xiang and G. D. Qian, *Acc. Chem. Res.*, 2010, **43**, 1115; (c) J. M.

- Zhou, W. Shi, H. M. Li, H. Li and P. Cheng, *J. Phys. Chem. C*, 2014, **118**, 416; (d) Z. M. Hao, X. Z. Song, M. Zhu, X. Meng, S. N. Zhao, S. Q. Su, W. T. Yang, S. Y. Song and H. J. Zhang, *J. Mater. Chem. A*, 2013, **1**, 11043.
9. (a) X. H. Zhou, L. Li, H. H. Li, A. Li, T. Yang and W. Huang, *Dalton Trans.*, 2013, **42**, 12403; (b) S. Dang, E. Ma, Z. M. Sun and H. J. Zhang, *J. Mater. Chem.*, 2012, **22**, 16920; (c) Q. Tang, S. X. Liu, Y. W. Liu, J. Miao, S. J. Li, L. Zhang, Z. Shi and Z. P. Zheng, *Inorg. Chem.*, 2013, **52**, 2799; (d) Z. H. Xiang, C. Q. Fang, S. H. Leng and D. P. Cao, *J. Mater. Chem. A*, 2014, DOI: 10.1039/C4TA00313F.
10. (a) R. Decadt, K. Van Hecke, D. Depla, K. Leus, D. Weinberger, I. Van Driessche, P. Van der Voort and R. Van Deun, *Inorg. Chem.*, 2012, **51**, 11623; (b) M. Ji, X. Lan, Z. P. Han, C. Hao and J. S. Qiu, *Inorg. Chem.*, 2012, **51**, 12389.
11. (a) N. Reimer, B. Gil, B. Marszalek and N. Stock, *CrystEngComm*, 2012, **14**, 4119; (b) H. Reinsch and N. Stock, *Micropo. Mesopo. Mater.*, 2013, **171**, 156.
12. P. Horcajada, C. Serre, D. Grosso, C. Boissiere, S. Perruchas, C. Sanchez and G. Ferey, *Adv. Mater.*, 2009, **21**, 1931.
13. (a) Y. Zhou and B. Yan, *CrystEngComm*, 2013, **15**, 5694; (b) X. H. He and B. Yan, *J. Mater. Chem. C*, 2013, **1**, 3910.
14. (a) B. R. Judd, *Phys. Rev.*, 1962, **127**, 750; (b) Y. Zhou, B. Yan and X. H. He, *J. Mater. Chem. C*, 2014, **2**, 848.
15. Y. Y. Liu, R. Decadt, T. Bogaerts, K. Hemelsoet, A. M. Kaczmarek, D. Poelman, M. Waroquier, V. Van Speybroeck, R. Van Deun and P. Van Der Voort, *J. Phys. Chem. C*, 2013, **117**, 11302.
16. (a) Z. C. Wen, R. Yang, H. He and Y. B. Jiang, *Chem. Commun.*, 2006, 106; (b) J. Y. An, C. M. Shade, D. A. Chengelis-Czegana, S. Petoud and N. L. Rosi, *J. Am. Chem. Soc.*, 2011, **133**, 1220.
17. S. W. Thomas, G. D. Joly and T. M. Swager, *Chem. Rev.*, 2007, **107**, 1339.
18. (a) C. X. Yang, H. B. Ren and X. P. Yan, *Anal. Chem.*, 2013, **85**, 7441; (b) M. Wang, J. G. Wang, W. J. Xue and A. X. Wu, *Dyes Pigm.*, 2013, **97**, 475; (c) X. F. Wu, B. W. Xu, H. Tong and L. X. Wang, *Macromolecules*, 2010, **43**, 8917; (d) A. J. Weerasinghe, C. Schmiesing, S. Varaganti, G. Ramakrishna and E. Sinn, *J. Phys. Chem. B*, 2010, **114**, 9413.
19. P. Y. Zhang, L. M. Pei, Y. Chen, W. C. Xu, Q. T. Lin, J. Q. Wang, J. H. Wu, Y. Shen, L. N. Ji and H. Chao, *Chem. Eur. J.*, 2013, **19**, 15494.
20. B. L. Chen, L. B. Wang, Y. Q. Xiao, F. R. Fronczek, M. Xue, Y. J. Cui and G. D. Qian, *Angew. Chem., Int. Edit.*, 2009, **48**, 500.
21. (a) M. Kim, J. F. Cahill, H. H. Fei, K. A. Prather and S. M. Cohen, *J. Am. Chem. Soc.*, 2012, **134**, 18082; (b) C. K. Brozek, A. F. Cozzolino, S. J. Teat, Y. S. Chen and M. Dinca, *Chem. Mater.*, 2013, **25**, 2998.